Multifrequency seashell antenna based on resonant cold-electron bolometers with kinetic Inductance Nanofilters for CMB measurements

Multifrequency seashell antenna based on resonant cold-electron bolometers with kinetic Inductance Nanofilters for CMB measurements

Cite as: AIP Advances 9, 015321 (2019); doi: 10.1063/1.5080323
Submitted: 7 November 2018 • Accepted: 7 January 2019 •
Published Online: 23 January 2019

A. S. Mukhin,[1,2] L. S. Kuzmin,[1,2,a)] A. V. Chiginev,[2,3] A. V. Blagodatkin,[2,3] V. O. Zbrozhek,[2] A. V. Gordeeva,[2,3] and A. L. Pankratov[2,3]

AFFILIATIONS

[1]Chalmers University of Technology, Department of Microtechnology and Nanoscience, SE-412 96 Gothenburg, Sweden
[2]Nizhny Novgorod State Technical University n.a. R.E. Alekseev, Nizhny Novgorod 603951, Russia
[3]Institute for Physics of Microstructures, Russian Academy of Sciences, Nizhny Novgorod 603950, Russia

[a)]**Correspondence email:** leonid.kuzmin@chalmers.se

ABSTRACT

A novel type of the seashell slot antenna with internal filters by the capacitance of resonant cold-electron bolometers (RCEB) and kinetic inductance of the NbN superconducting nanostrip has been realized for multifrequency pixels. Seashell antenna gives the opportunity to connect opposite slots by coplanar waveguides (CPW) instead of microstrip lines (MSL). A conventional multifrequency pixel combines a wideband antenna and narrowband filters with long microstrip lines with unavoidable losses and overlaps. Another problem is the frequency dependent beam width due to a fixed pixel diameter for multiple frequencies. The main advantage of the seashell antenna with nano-filters is independent tuning of the separate pairs of slots for each frequency avoiding frequency dependence of the beam width. We used $\lambda/2$ slots for 75 and 105 GHz, feeding by CPW near the end of slots for RF matching. Each RCEB includes two SIN (Superconductor-Insulator-Normal) tunnel junctions with a nano-absorber and NbN kinetic inductance of 450 or 310 pH. SIN junctions had capacitances of 9.3 and 7.2 fF and absorber matched to a wave impedance of the antenna near 50 Ohm. Kinetic inductance value was estimated at the level of 35 pH/sq. RF testing was done at 300 mK irradiating this chip by sweep generator from 60 to 120 GHz. The response curves showed clear resonances at 75 and 105 GHz with a quality factor of 10 and 7. These experiments confirm that the seashell antenna with the internal RCEB filters can be used for frequency selection in compact multiband pixels.

Recent discoveries[1,2] in the study of cosmic microwave background (CMB) radiation have stimulated interests to detector technology. Superconducting bolometers at sub-Kelvin temperatures can achieve sensitivity limited by fluctuations in the arrival photons. However, observation of celestial features by space telescopes would considerably benefit from simultaneous data acquisition by colocated multifrequency detector arrays.[3–5]

The benefit of multichroic systems comes from the ability to characterize the foreground signals of celestial objects. CMB polarization measurements require spectral information to remove polarized galactic foregrounds based on spectral signatures.[3,4] A potential future B-mode CMB mission, like COrE (Cosmic Origins Explorer),[5] adding full dual-polarization capability and an increased number of pixels as compared with the Planck instrument, could be based on multifrequency focal plane arrays able to operate at various (sub)mm-wave bands and dual polarizations.

A conventional concept of the multichroic system is a combination of the wideband sinuous antenna or horn-coupled detectors and narrowband filters comparable with a wavelength.[4,5] However, this system is quite large and

includes long microstrip lines with unavoidable losses. A common problem with a conventional multichroic pixel, which has a single pixel diameter, is that the beam width and the optimal pixel diameter are frequency dependent.[6] It is usually impossible to choose a pixel diameter that is optimal in every frequency band.

The most effective way for the size reduction would be the development of a novel type of bolometer with internal bandpass filters instead of external on-chip filters. The best candidate for this goal is a capacitively coupled cold-electron bolometer (CEB)[7–9] based on self-cooling by SIN tunnel junctions. Besides high sensitivity and wide dynamic range CEBs demonstrate immunity to cosmic rays due to the tiny volume of the absorber and decoupling of the phonon and electron subsystems.[10] For frequency selection, we used the resonant cold-electron bolometer (RCEB)[11] with internal nanofilter organized by a kinetic inductance of the NbN superconducting nanostrip and a capacitance of the nanoscale SIN tunnel junction (Fig. 1). The RCEB allows reducing size of the inductance up to 300 times compared to the geometrical inductor of the same inductance. This internal resonance has a bandwidth of 5-20% needed for radioastronomy applications. The RCEB concept was proved using a single Lambda slot with two RCEBs for 75 and 105 GHz.[12]

In the present Letter, we have realized a multichroic system based on the seashell antenna and RCEB with NbN kinetic inductance in scopes of a European Space Agency Technical Research Programme (TRP) investigating architectures for focal plane configurations suitable for future space missions such as COrE to detect the B-mode of the CMB.[5]

As a promising candidate of the multichroic systems, a novel "seashell" slot antenna has been proposed for this goal.[13,14] The seashell antenna has several advantages compared to multichroic sinuous[4,6] and cross-slot[5] antennas. The main advantage of the seashell antenna is the opportunity to tune independently separate pair of slots for each frequency. The design of the one polarization seashell antenna for 75 and 105 GHz is shown in Fig. 2a. The antenna consists of two pairs of slots separated by $\lambda/2$ to form the required beam characteristics. The slot antennas are connected by CPWs instead of MSLs that has several advantages. The most important for technology is that the design with CPW requires less number of layers (one layer instead of three layers) and it is impossible to use CPW for sinuous antenna because of unavoidable overlap of MSLs (+2 layers). CEB is inserted into the central wire of the CPW and shown by red triangles in Fig. 2a.

To form a proper beam shape, the slots must be placed at $\lambda/2$ distance. We have introduced narrowing of the slots in the middle part creating lumped capacitance to make the

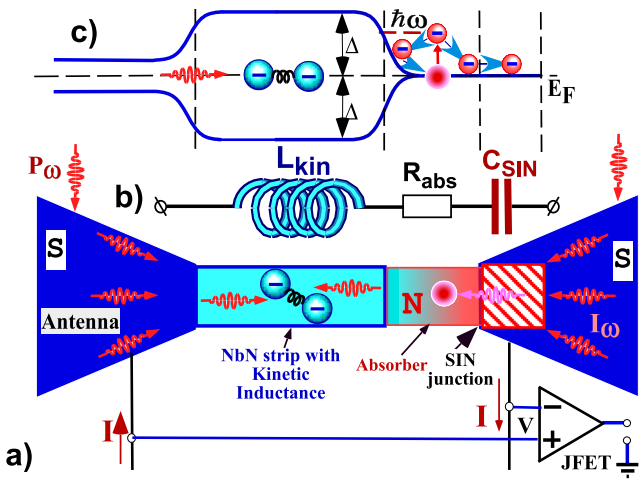

FIG. 1. a) Sketch of the **Resonant Cold-Electron Bolometer (RCEB)** with kinetic inductance of the superconducting NbN strip and capacitance of the SIN tunnel junction as an RF internal filter, b) equivalent scheme of RCEB and c) energy diagram of RCEB with $\Delta > hf$.

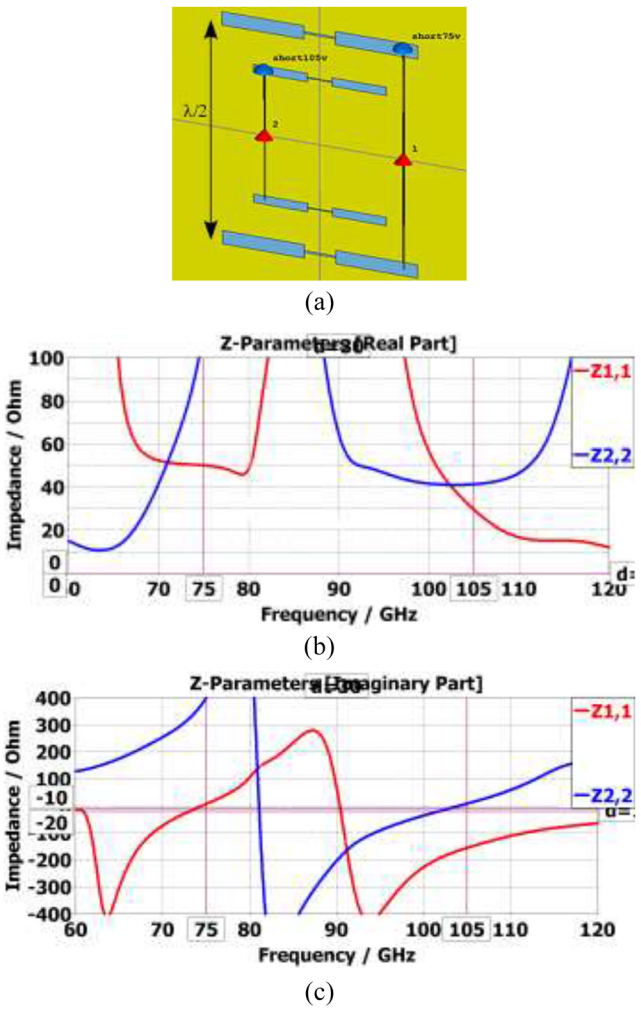

FIG. 2. The design of the multichroic seashell antenna for one polarization. (a) A view in CST Microwave Studio; the blue parts are holes in a yellow ground plane (b) ReZ and (c) ImZ of the seashell antenna vs frequency for 75 GHz (red) and 105 GHz (blue) channels.

slot length shorter by keeping the same electrical length. The impedance of λ/2 slot antenna is relatively high in the middle of slots. Displacing the feeding point closer to the edge lead to lower impedance to match a slot to CPW. The total resonant system is formed by the slot antenna with CPW, the capacitance of CEB, the resistance of absorber and the inductance of NbN microstrip.

Estimation of NbN inductance were made in Ref. 14 using a simple slot antenna CEB with NbN strip inside the slot. Here we need to consider a total antenna system with CPW. The DC biasing of CEB is provided through coplanar lines by DC connectors, which are located under the ground plane and shown by blue triangles in Fig. 2a. The influence of the DC connectors on the electrodynamics of the antenna is taken into account by the effective capacitances between connectors and ground plane, estimated as 350 fF.

The numerical modeling of the two-frequency seashell antenna is performed in CST Microwave Studio. The electrodynamical part of the calculations is made by two solvers – time domain and frequency domain. The comparison of the results obtained by these two solvers demonstrates their similarity.

Fig. 2b, c shows the real and imaginary parts of the antenna impedance vs frequency. From the electrodynamics part of calculations, we obtain the values of diagonal components of the Z matrix at operating frequencies 75 and 105 GHz. Here ReZ_{11}(75 GHz) = 50 Ohm, ImZ_{11}(75 GHz) = 6.7 Ohm, ReZ_{22}(105 GHz) = 48 Ohm, and ImZ_{22}(105 GHz) = 8.5 Ohm. Then we use these values to create the required resonances at operating frequencies with schematics shown in Fig. 3. The equivalent circuit of RCEB connected to a seashell antenna (Fig. 3a) is an LCR circuit, where the resistance of a port corresponds to the resistivity of the CEB absorber R_{abs}, and the capacitance corresponds to the total capacitance of two SIN junctions of the CEB connected in series C_{SIN}= C_{SIN1}/2. The equivalent circuit of the seashell antenna with CPW consists of the imaginary part of the antenna impedance ImZ_e including the capacitance C_e, inductance L_e, and the real part of the antenna impedance ReZ_e connected in series (Fig. 3a). Here L_e is determined by the slope of ImZ:

$$L_e = \frac{1}{4\pi}\frac{dImZ}{df}, \quad C_e = \frac{1}{4\cdot\pi^2 f^2 L_e}, \tag{1}$$

at the frequency of series resonance where ImZ=0 at f_s~75 GHz and f_s~105 GHz, see Fig. 3b. L_e = 2.7·10^{-9}H and C_e = 1.5·10^{-15}F for 75GHz and L_e = 1.6·10^{-9}H and C_e = 1.6·10^{-15}F for 105GHz.

Spectral characteristics of the seashell antenna with two CEBs are obtained (Fig. 3c). The values of L_{kin}, R_{abs} and C_{SIN} are the following: L_{kin}=450 pH, R_{abs}=54 Ohm, C_{SIN}=9.3 fF for 75 GHz and L_{kin}=310 pH, R_{abs}=37 Ohm, C_{SIN}=7.2 fF for 105 GHz. From Fig. 3 the widths of the resonances are nearly 11.2 GHz for 75 GHz and 12 GHz for 105 GHz. There are parasitic resonances at frequency of 106 GHz in 75 GHz channel and frequency of 66 GHz in 105 GHz channel. The maximal cross-talk of the antenna -13 dB is reached around 105 GHz (green dashed curve in Fig. 3c).

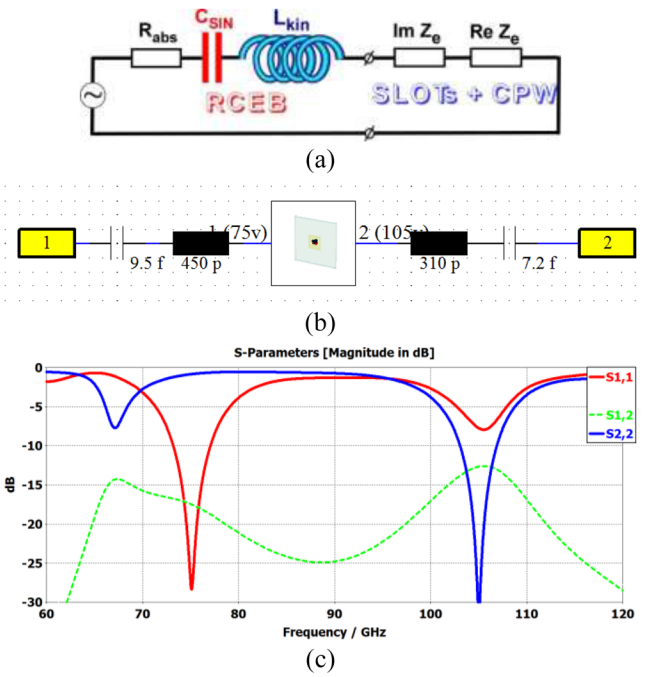

FIG. 3. (a) Equivalent circuit of the seashell antenna connected to a CEB with NbN kinetic inductance, (b) the equivalent circuit used in the numerical modelling and (c) frequency characteristics of the system tuned to 75 (red) and 105 GHz (blue).

Fabrication of RCEB is a 5-layer process. The first layer "thin gold" is made of 1nm titanium adhesion layer, 15nm gold and 2nm palladium layer for contact between gold and aluminum electrodes. The pattern is formed by optical laser lithography and e-beam evaporation. Functionally this layer forms the contact area to bolometer and DC wiring. The second layer is an insulation of 40nm by Silicon dioxide between wiring and ground plane. The capacitive area formed by overlapping of thin gold wiring and the ground plane level was made big enough to no introduce any impact at a total characteristic of the device at the working frequencies.

The third layer is NbN strips of 20nm fabricated by magnetron sputtering of niobium in a nitrogen atmosphere (Fig. 4). The width of the NbN strip was chosen to be 2um to be able to fabricate it using optical lithography. The inductive impact was regulated by changing the length of the micro strip line. To achieve desired values of L_{kin}=450pH and L_{kin} =310pH for 75GHz and 105GHz channels respectively the total length of 25um and 17um.

A fourth layer is a ground plane made of 10nm of Ti, 180nm of gold and 20nm of Pd. The critical dimensions on that level are the sizes of a micro strip lines. The designed width of the middle electrode supposed to be 2um and the gap between the centre electrode and the ground plane 2um. However in the real fabricated device we had a wider central electrode with is a potential source of misalignment with predicted properties. The last sixth layer is CEB fabricated by a self-aligned shadow evaporation technology[15] (Fig. 4, insert). This is the only layer

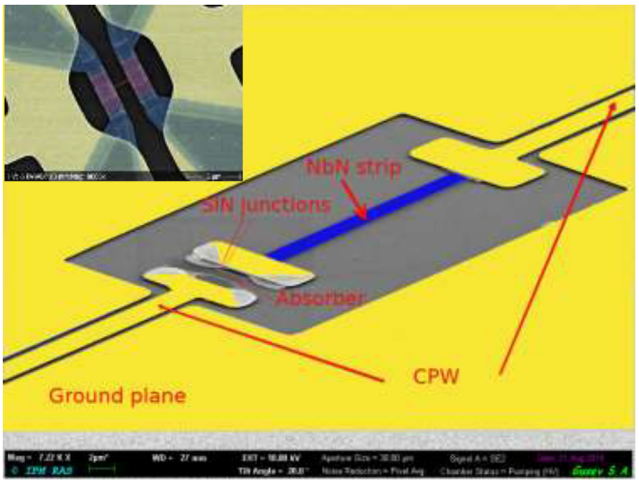

FIG. 4. SEM image of the CEB with NbN strip; inset: CEB comprising two SIN tunnel junctions (pink) and an absorber (red).

that requires a the patterning with sage of e-beam lithography. A layer of normal metal (20nm aluminum with 1nm of iron for suppression of superconductivity), insulator, and top superconducting electrodes form the CEB. Insulation was made by oxidising aluminium in a pure oxygen atmosphere at a pressure of 10 Tor for 10 minutes. Aluminium electrodes of 50 nm were deposited at +/-45 angles. The whole bolometer with needed area of tunnel junctions was fabricated in the same chamber without breaking the vacuum.

To get a total capacitance of 7.2 fF for 105GHz and 9.3fF for 75GHz frequency channels we used junctions of 1.4μm x 0.2μm and 1.4μm x .280 μm from $C_{junction} = \frac{50fF}{sq.\mu m}$. The structure of CEB implies a series connection of two SIN junctions and $C_{total} = C_{sin}/2$.

The inductance was realized by microstrip of NbN. Generally, the inductance of NbN can be defined as

$$L_k = \frac{\mu_0 l}{w}\frac{L^2}{b}, \tag{2}$$

where w, b are width and thickness and l is length of a strip. L is a magnetic penetration depth defined as

$$\mathbf{L}^{-2} = \frac{\pi\mu_0 \boldsymbol{\Delta}}{\hbar \boldsymbol{\rho}}, \tag{3}$$

where Δ is a superconducting energy gap and ρ is normal state resistivity. For our process, we proved that fabrication of 20 nm films could be well reproducible without degradation of film properties. The value of kinetic resistance at the level of 35 pH/sq was proven by measuring a resonant frequency of LRC circuits formed by NbN strip capacitance of CEB integrated into an L/2 slot antenna.[12] That experiment proved that kinetic inductance can be properly estimated by indirect measurements of T_c and surface resistance of NbN film.

One of the biggest challenges in fabrication was a minimization of parasitic contact resistance of NBN and gold pads. To minimize the resistance we made a sandwich of the first layer of gold, NbN contact area, and the fourth layer of gold. This approach of creating a contact interface Au-NbN-Au helped to avoid parasitic contact resistance.

For measuring the RF response of the sample, the IV curves of the CEBs were measured in the absence of an external signal.[16,17] Then a radiation source at a frequency of 75 GHz or 105 GHz was switched on, and the I-V curves of structures were measured compared with the autonomous I-V curves. Selecting the optimal bias point for a maximum response then the sample was irradiated by a sweep generator from 60 to 120 GHz. Measurement of a frequency response through the window of a cryostat is a non-trivial task. The main problem is standing waves inside the cryostat. For compensation of standing waves, we discovered that simultaneous measurement of two frequency channels gives the best result. Simultaneous spike or deep on both channels is a visible indication that we see an external resonance or standing waves.

To minimize that disturbing effect of standing waves we used the following approach, which can be called space averaging. Nine cells connected in series were placed on the chip (Fig. 5a). The total response could be measured from all nine cells together. In this case, if one of the cells is in the node of the standing wave at a given frequency, the effect of this influence will be nine times less. Combined with time averaging it gives us more smoothed response curves.

Fig. 5 shows the frequency the pure normalized measured response of the sample (solid curves) with six cells (Fig. 5b) and three cells (Fig. 5c). The thick dashed lines level is a detector bias point which in this experiment is equal to the dark (closed optical window) signal level. While making the measurements with a sweep generator the RF signal power was tuned to be as low enough not to introduce the heating of the substrate. While regulating the RF power, we observed a rise of response signal uniformly within the range of the generator, while the response shape remained unchanged which is the indicator of a substrate heating effects. Since the measurements of the resonant curves were made simultaneously for both frequency pixels, the most important date, that one can notice is that maximum coupling for one pixel corresponds to rejection frequency for another pixel. The red curve shows the resonance corresponding to the 75 GHz channel, the blue curve - 105 GHz channel and the dashed curves show the results of theoretical fitting. One can see good qualitative agreement between theory and experiment with multichroic band-pass filters for these two frequencies. However, the measured resonant frequencies are slightly lower than the designed frequency of 75 and 105 GHz. Certain disagreement in central frequencies and bandwidths may be due to a mismatch in the antenna and CPW size at the stage of lithography. The frequency shift can also be affected by the size of tunnel junctions since the capacitance of the SIN junctions is proportional to the area of junctions. In total, the following results were demonstrated in the experiment. For 75 GHz pixel, the central frequency is in perfect correspondence with a designed value of 75GHz for the first sample Fig 5b and shifted down for 6-7 GHz against the designed value for the second sample Fig 5c.

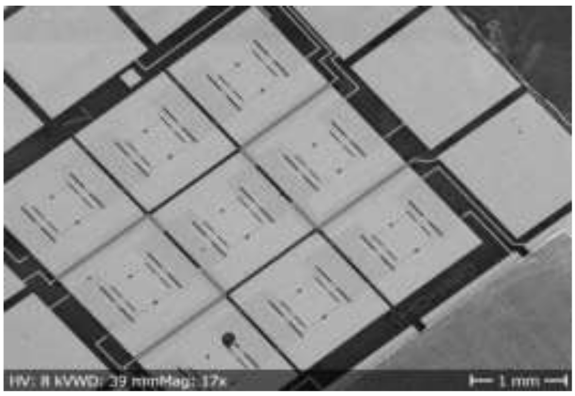

(a)

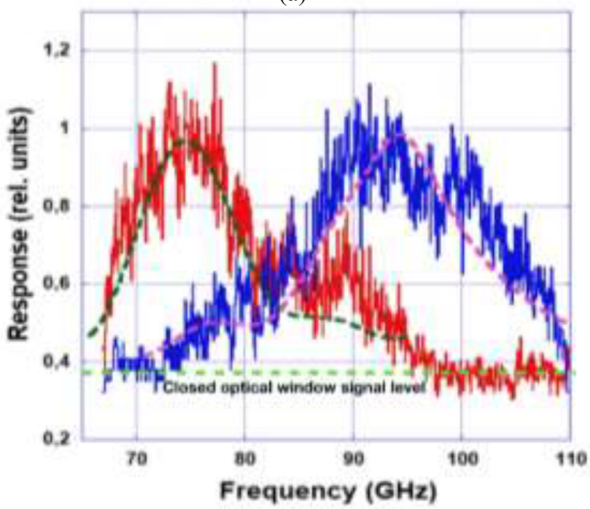

(b)

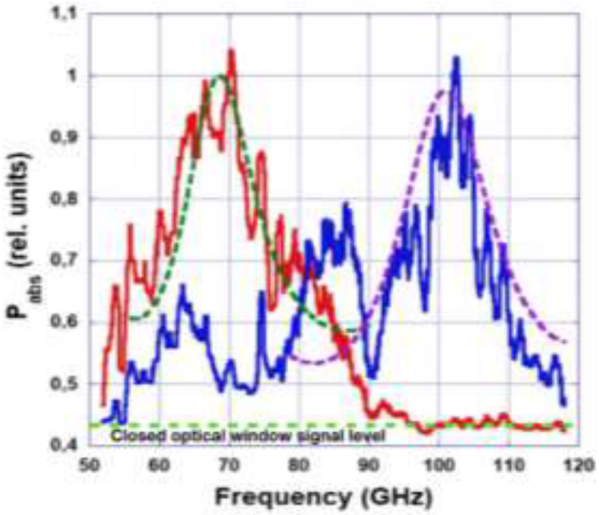

(c)

FIG. 5. (a) Chip layout with nine cells of the seashell antenna with RCEBs, connected in series. (b) The measured response of six cells to the RF signal for 75 GHz (red) and 105 GHz (blue) channels and the theoretical fitting curves (dashed curves); (c) the same for three cells connected in series.

The bandwidths estimated at the level of 0.5 by power are BW = 7 GHz (Q = 10.7) for the first sample and BW = 9 GHz (Q = 7.6) for the 75 GHz channel. For the 105 GHz channel we achieved a bandwidth of BW = 11 (Q = 8.5) and BW = 11GHz (Q = 9.2) for the first and the second sample respectively.

In summary, we have successfully demonstrated the operation of a novel multifrequency seashell antenna with internal bandpass filters by the capacitance of cold-electron bolometers and kinetic inductance of NbN strips. This structure gives a unique opportunity to tune independently each frequency band determined by double slot and CEBs with NbN strips. Contrary to a conventional multifrequency sinuous antenna with TESs and horn-coupled multichroic detectors connected by long microstrip lines with unavoidable losses and overlaps, the seashell antenna could use the independent coplanar line for each frequency band fabricated by a single-layer technology. Besides that, the seashell antenna gives a critical opportunity to keep the beam width of the same size for different frequency bands due to the independent tuning of a beam by the corresponding pair of phased slots for each frequency.

The authors would like to thank the team of the ESA Project AO/1-7256/"Next Generation Sub-millimetre Coupling Concepts" for stimulating discussions, A. Sobolev and S. Mahashabde for discussions and CST simulations, and M. Tarasov for assistance in fabrication of samples. Samples were fabricated in Chalmers Nanotechnology Center, sample measurements were performed at Chalmers University of Technology and the Center of Cryogenic Nanoelectronics of NNSTU. The work is supported by the ESA TRP Project No. 4000109434/13/NL/MH and the Ministry of Education and Science of Russia (Project 16.2562.2017/PCh).

REFERENCES

[1] C. Seife, Science **302**, 2038–2039 (2003).
[2] J. A. Grayson, P. A. R. Ade, Z. Ahmed, K. D. Alexander, M. Amiri, D. Barkats, S. J. Benton, C. A. Bischoff, J. J. Bock, H. Boenish *et al.*, Proc. SPIE **9914**, 99140S (2016).
[3] R. O'Brient, P. Ade, K. Arnold, J. Edwards, G. Engargiola, W. L. Holzapfel, A. T. Lee, M. J. Myers, E. Quealy, G. Rebeiz *et al.*, App. Phys. Lett. **102**, 063506 (2013).
[4] J. McMahon, J. Beall, D. Becker, H. M. Cho, R. Datta, A. Fox, N. Halverson, J. Hubmayr, K. Irwin, J. Nibarger, M. Niemack, and H. Smith, J Low Temp Phys. **167**, 879–884 (2012).
[5] N. Trappe *et al.* (+23 authors), Proc. SPIE **9914 VIII**, 991412L (2016).
[6] A. Cukierman, A. T. Lee, C. Raum, A. Suzuki, and B. Westbrook, Appl. Phys. Lett. **112**, 132601 (2018).
[7] L. Kuzmin, Proceedings of the International Workshop on Superconducting Nano-Electronics Devices, 145 (2001); L. Kuzmin and D. Golubev, Physica C **372-376**, 378 (2002).
[8] L. Kuzmin, Journal of Physics: Conference Series (JPCS) **97**, 012310 (2008).
[9] M. Tarasov, L. Kuzmin, V. Edelman, and P. de Bernardis, IEEE Trans. on Applied Superconductivity **21**, 3635 (2011).
[10] M. Salatino, P. de Bernardis, L. S. Kuzmin, S. Mahashabde, and S. Masi, J. Low Temp. Phys. **176**, 323 (2014).
[11] L. S. Kuzmin, IEEE Trans. on Terahertz Science and Technology **4**, 314 (2014).
[12] L. S. Kuzmin, A. S. Mukhin, and A. V. Chiginev, IEEE Transactions on Applied Superconductivity **28**, 2400304 (2018).

[13]L. S. Kuzmin, A. V. Chiginev, E. A. Matrozova, and A. S. Sobolev, IEEE Transactions on Applied Superconductivity **26**, 2300206 (2016).
[14]L. S. Kuzmin and A. V. Chiginev, Proc. SPIE **9914**, 99141U (2016).
[15]L. S. Kuzmin, "Self-aligned shadow evaporation technology for large area tunnel junctions and nanoabsorbers," Journal of Vacuum Science and Technology (to be submitted).
[16]A. V. Gordeeva, V. O. Zbrozhek, A. L. Pankratov, L. S. Revin, V. A. Shamporov, A. A. Gunbina, and L. S. Kuzmin, Appl. Phys. Lett. **110**, 162603 (2017).
[17]L. S. Kuzmin, V. A. Shamporov, A. A. Gunbina, A. L. Pankratov, A. V. Gordeeva, V. O. Zbrozhek, S. Masi, and P. De Bernardis, IEEE Xplore Proc. of 16th International Superconductive Electronics Conference (2018).